JACS
JOURNAL OF THE AMERICAN CHEMICAL SOCIETY

ARTICLE

pubs.acs.org/JACS

Highly Sensitive and Selective DNA-Based Detection of Mercury(II) with α-Hemolysin Nanopore

Shuang Wen,[†,‡] Tao Zeng,[§,‡] Lei Liu,[†] Kai Zhao,[†] Yuliang Zhao,[*,†,§] Xianjin Liu,[∥] and Hai-Chen Wu[*,†]

[†]Key Laboratory for Biomedical Effects of Nanomaterials & Nanosafety, Institute of High Energy Physics, Chinese Academy of Sciences, Beijing 100049, China

[§]National Center for Nanoscience and Technology of China, Beijing 100190, China

[∥]Key Lab of Food Quality and Safety of Jiangsu Province-State Key Laboratory Breeding Base, Key Lab of Agro-Food Safety and Quality, Ministry of Agriculture, Institute of Food Safety, Jiangsu Academy of Agricultural Sciences, Nanjing 210014, China

Supporting Information

ABSTRACT: The duplex formation mediated by Hg^{2+} in a properly designed ssDNA generates a stable hairpin structure, which greatly alters the translocation profile of the ssDNA through α-hemolysin nanopore. From the 2D-events contour plot, the presence of Hg^{2+} can be confirmed in as little as 30 min at ~7 nM or higher. The sensor is highly selective to Hg^{2+}, without interference from other metal ions. It can be fabricated from readily available materials, without the processes of synthesis, purification, probe-making, and so forth. This sensing strategy opens new possibilities for detecting many types of analytes which have specific interactions with DNA molecules.

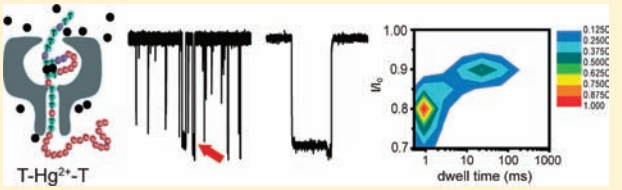

INTRODUCTION

Mercury, present in a variety of different forms (metallic, inorganic, and organic), is a widespread bioaccumulative pollutant. Mercury not only appears in industrial operations, but also exists in our lives such as batteries, thermometer, cosmetics, food, and water.[1−3] In recent years, water pollution is regarded as one of the major environmental concerns. Solvated mercuric ion (Hg^{2+}), one of the most stable inorganic forms, draws special attention, as Hg^{2+} is a neurotoxin and can cause severe adverse effects on human health through food-chain accumulation or high dose exposure.[4−8] Thus, a convenient and sensitive detection of Hg^{2+} is central to the environmental monitoring of natural water resources and aquatically derived food safety.

So far, numerous techniques have been reported for Hg^{2+} detection by employing fluorophores,[9] chromophores,[10] gold nanoparticles,[11] single-walled carbon nanotubes,[12] semiconductor nanocrystals,[13] polymers,[14] cyclic voltammetry,[15] microcantilevers,[16] DNAzyme,[17] and so forth. Recently, a Hg^{2+}-specific thymine−thymine (T−T) base pair has shown its power in the design of sensitive Hg^{2+} sensing platforms. Ono developed a T-rich DNA fluorescence probe functionalized with a fluorophore and a quencher at 3′ and 5′ ends, respectively.[18] Introduction of Hg^{2+} brought the fluorophore and quencher moieties close to each other and thus quenched the fluorescence. Colorimetric detection of Hg^{2+} using DNA-functionalized gold nanoparticles and DNA-based machines was also reported.[11a,c] Hg^{2+}-mediated DNA duplex formation triggered the color change of the probes and thus realized the detection. On the basis of a similar rationale, a highly sensitive and selective catalytic beacon derived from a uranium-specific DNAzyme[19] and regenerable DNA-functionalized hydrogels were developed for Hg^{2+} detection and removal.[20]

Single-channel electrical recording has proven to be a powerful tool in molecules detection. Bayley's group pioneered in the stochastic sensing of various analytes, such as metal ions,[21] proteins,[22] DNA,[23] and organic molecules,[24] using an α-hemolysin (αHL)-based nanopore system. When an analyte binds within the protein pore, the ionic current will be modulated and current fluctuation events can be recorded. The frequency of the events reveals the concentration of an analyte and the characteristic current signature reveals its identity. For most molecular sensing activities, engineered αHL pores or adapters are required to provide the binding elements. Braha and colleagues reported simultaneous detection of three different divalent metal ions with a single sensor element inside an αHL mutant.[21] However, this elegant but somewhat serendipitous work is difficult to imitate. Recent protein nanopore-based researches include single-molecule chemistry studies,[25] monitoring the conformational change of biomolecules inside the nanopore cavity,[26] and others mainly focused on single-molecule nanopore DNA sequencing.[27] Herein, we present a highly sensitive and selective detection method for Hg^{2+} with αHL-based single-channel recording in the presence of deliberately designed DNA oligomers.

RESULTS AND DISCUSSION

Prompted by the successful applications of the T−Hg^{2+}−T pairing (Figure 1A) and the wealth of information about single-stranded

Received: July 26, 2011
Published: October 13, 2011

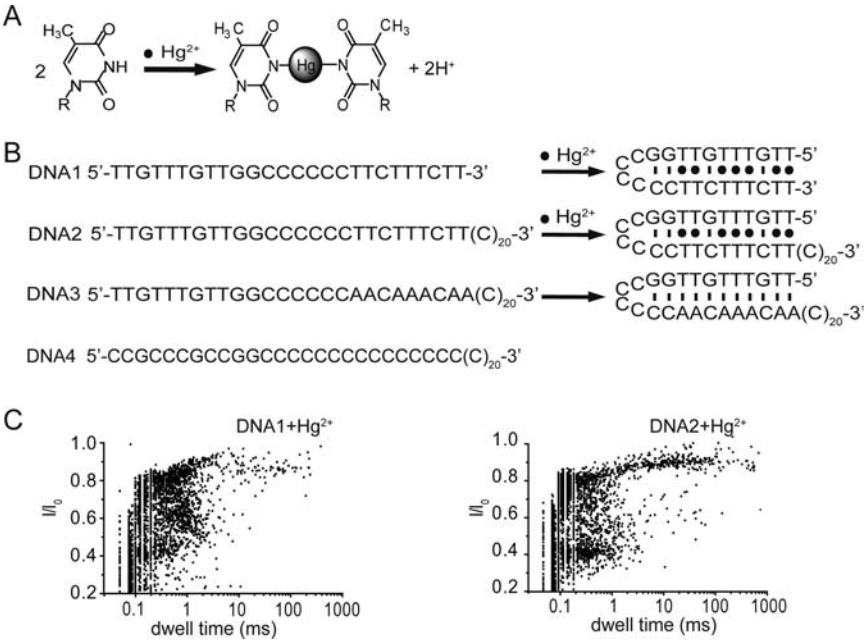

Figure 1. Design of DNA sequences for Hg^{2+} detection. (A) Reaction scheme of Hg^{2+} binding with thymine base pairs. (B) Sequences of DNA1−4. Upon Hg^{2+} binding, DNA1 and DNA2 can form hairpin structure through Thymine−Hg^{2+}−Thymine pairing; DNA3 forms natural hairpin through Watson−Crick base pairs; DNA4 is a control with low secondary structure. (C) Scatter plot of the events (normalized current blockage I/I_0 versus event durations) caused by DNA1 and DNA2 (DNA final concentration 1.0 μM), respectively, in presence of 7.0 μM Hg^{2+} in 1 M KCl, 25 mM Tris, pH 8.0 buffer (number of individual experiments n = 5).

DNA (ssDNA) translocated through αHL nanopore, we envisioned that a simple but efficient Hg^{2+} sensor could be fabricated with readily available materials. The duplex formation within a ssDNA mediated by Hg^{2+} would generate a stable hairpin structure on the strand (Figure 1B), which might greatly alter the translocation profile of the ssDNA. To test this hypothesis, a 26-base T-rich nucleic acid (DNA1, Figure 1B) was designed for Hg^{2+} detection according to literature.[18] Indeed, in a single-channel recording with αHL WT-D8H6 at +100 mV (for preparation of αHL and single-channel recording conditions, see Experimental Section), a large number of events with prolonged dwell time appeared outside the normal ssDNA translocation region in the presence of 7.0 μM Hg^{2+} (Figure 1C). The occurrence of these long events is very likely due to the duplex formation of DNA1 mediated by 7 T-Hg^{2+}-T pairs and 4 guanine−cytosine (G−C) pairs, which necessitates the unzipping process prior to translocation. Considering a hairpin-shaped nucleic acid with a single-stranded overhang might ease the unzipping process during the DNA translocation to afford more discernible signals,[28,29] we added a 20-base poly(C) tail to the 3′-end of DNA1 to become DNA2. DNA2 was then tested in the same experiment under identical conditions. A new cluster with a distinct boundary in the scatter diagram can be readily distinguished. We also tried some other nucleic acids (DNA5−7, Supporting Information Table S1), but none of them gave better results than DNA2 (see Figure S1 for examples).

With the initial success in hand, we set out to fully investigate and evaluate this strategy for Hg^{2+} detection. Figure 2A shows the results of a control experiment, that is, DNA2 translocation in the absence of Hg^{2+}. The DNA with random coil conformation gives an average current blockage of ∼80% and the most probable translocation time (t_p) of 0.16 ± 0.01 ms (n = 8). Figure 2B illustrates the unzipping and translocation of DNA2 in the presence of 7.0 μM Hg^{2+}. A large number of markedly prolonged events could be observed in the current trace (∼24 ms in Figure 2Bc). The average residual current drops to ∼10% of the open pore current and the t_p increases to 10−30 ms (n = 8). More prominently, a new region is generated on the 2D event-distribution contour map which unambiguously indicates the presence of Hg^{2+} in solution (Figure 2Bd). To compare the translocation profile of the T−Hg^{2+}−T stabilized hairpin with natural Watson−Crick base pair hairpin, we replaced half of the T in DNA2 with adenine (A) to form DNA3 (Figure 1B). The unzipping and translocation of DNA3 through αHL was carried out under the identical conditions. The scatter plot data shown in Figure S2 further supports the analogy of hairpin formation of natural A−T base pairs and T−T mismatches mediated by Hg^{2+}. The current blockage is slightly larger (∼5%) than that of free DNA2 and the translocation time lies within the range of 2−10 ms, in good agreement with literature values.[29] On the 2D contour map, A−T hairpin translocation produces an explicit but inseparable area. To be sure that the results shown in Figure 2B are exclusively effected by the T−Hg^{2+}−T pairing, we performed another control experiment with DNA4, which was designed by replacing all the T in DNA2 with C. The translocation of DNA4 through αHL was conducted in the presence of 7.0 μM Hg^{2+} under the standard conditions. The results are in close approximation to that in Figure 2A, confirming the role that the T−Hg^{2+}−T pairings play in the Hg^{2+} detection (Figure S3).

It is known that the transmembrane potential has a profound effect on the translocation of DNA molecules.[28,30] Thus, we carried out the Hg^{2+} detection experiments with DNA2 at different potentials (Figure S4A). When potentials are lower than +100 mV, the translocation events become scarce even for an hour recording (∼600 events/1 h at 80 mV; ∼1000 events/1 h at 90 mV; ∼1600 events/1 h at 100 mV). With the increase of

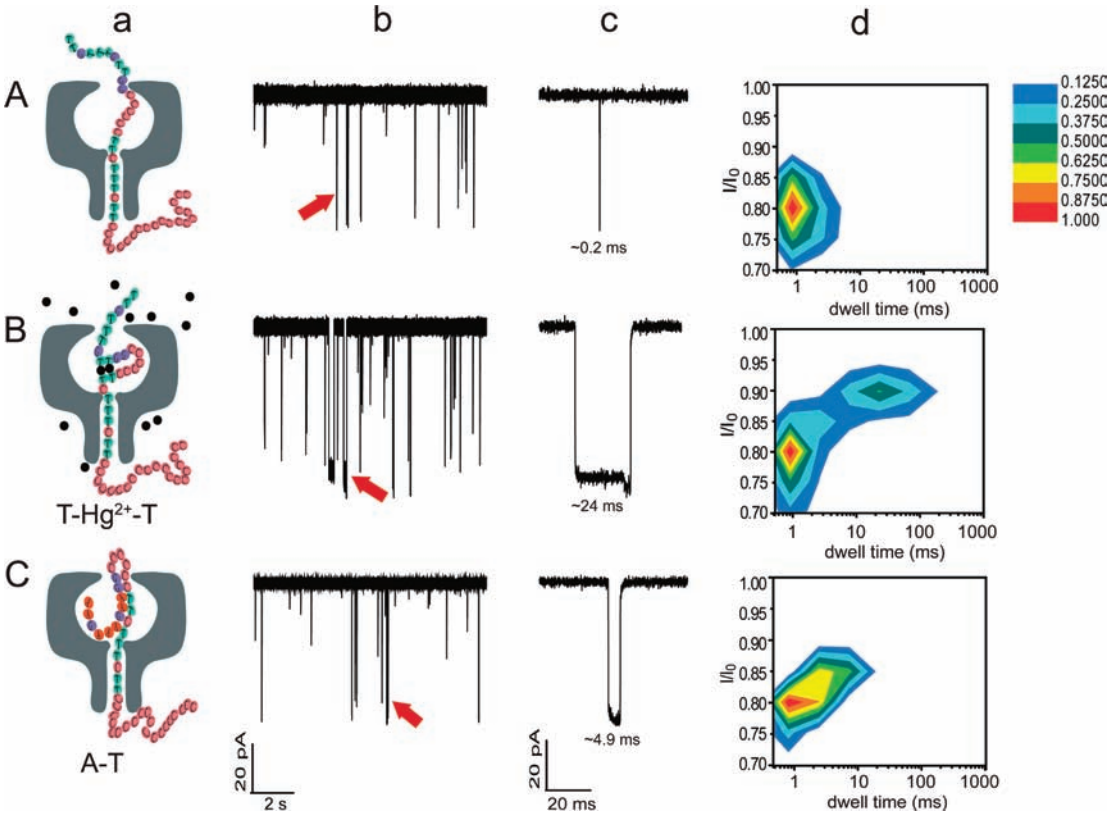

Figure 2. Representation of the translocation of ssDNA (DNA2), T−Hg^{2+}−T containing DNA hairpin (DNA2−Hg^{2+}), and natural DNA hairpin (DNA3) through a single αHL nanopore. [A−C] (a) Schematic illustration of DNA2, Hg^{2+}−DNA2, and DNA3 passing through αHL. [A−C] (b) Representative single-channel current traces of the translocation of DNA2, Hg^{2+}−DNA2, and DNA3. [A−C] (c) Expanded view of the events indicated in the current trace by a red arrow. [A−C] (d) Corresponding 2D event-distribution plots associated with DNA2, Hg^{2+}−DNA2, and DNA3 translocation through the pore. The distribution of events is plotted according to current blockage ($I/I_0 > 0.70$) and dwell time ($\tau_{off} > 300\ \mu s$). The density of events at each coordinate is indicated by the color code. All experiments were conducted in the buffer of 1 M KCl and 25 mM Tris, pH 8.0, with the transmembrane potential held at +100 mV. DNA1 and DNA2 (DNA concentration 1.0 μM) were preincubated with Hg^{2+} (final concentration 7.0 μM) for 1 h at room temperature before addeing into cis chamber. DNA3 was annealed at 95 °C for 3 min and slowly cooled to room temperature prior to use. The number of individual experiments $n = 5$.

the potential, the translocation time t_p decreases considerably (Figure S4B). So as to enhance the detection confidence with the new strategy, we chose +100 mV as the standard potential because most distinct difference can be observed on the 2D-events contour map at this value (Figure 2Bd).

A method adapted from literature[31] was used to conduct the quantitative analysis of Hg^{2+}. Scatter plot showing current blockage and dwell time is depicted in Figure 3A. An oval, specified as "Hg^{2+} signal region", was drawn to contain >95% of the translocation events of the Hg^{2+}-stabilized DNA2. It should be noted that only the events with current blockage greater than 70% were selected to constitute the "Hg^{2+} signal region", as the short partial blockades were proposed to be associated with DNA molecules colliding with, but not fully translocated through the pore.[31] Also, to avoid the intervention of normal ssDNA translocation, the events with duration less than 3 ms were chopped off for plotting an optimized signal region (Figure 3A; for unedited data, see Figure S5). The oval could also be used as a boundary to count the number of events derived from the translocation of Hg^{2+}-stabilized DNA2 hairpin. The number of events located in the signal region was then divided by the total number of DNA translocation events to give a probability, P_{Hg}, which should be associated with the concentration of Hg^{2+}. Almost no events of normal ssDNA translocation (without Hg^{2+}) fell into this region, indicating little interference from the background noise (Figure 3B; for unedited data, see Figure S5). Experiments with various concentration of Hg^{2+} were carried out under otherwise identical conditions. The results are shown in Figure 3C. The existence of Hg^{2+} can be unambiguously confirmed at ~0.7 μM or higher (indicated with an arrow in inset).

The detection limit of other sensors based on T−Hg^{2+}−T pairing typically ranges from few nM to about 100 nM.[11a,c,18−20] Our sensing system exhibits relatively low sensitivity due to two possible reasons. First, the background noise of DNA translocation is relatively high, especially when the metal concentration is low. Those prolonged events in the control experiments, which are indistinguishable from Hg^{2+}-mediated hairpin translocation events, are detrimental for detecting low concentration Hg^{2+}. Second, it is known that Cl^- can bind Hg^{2+} to decrease its effective concentration.[32] In our experiments, the salt solution contains 1 M Cl^-, which might deteriorate the effect when the concentration of Hg^{2+} is very low. Therefore, we sought to improve the sensitivity of the sensor using different strategies. Initial attempt to lower the KCl concentration to 0.1 M was not successful due to the low signal-to-noise ratio (Figure S6). We then tried to use a noncoordinating anion salt KNO_3 to weaken the binding effect. However, KNO_3 itself has a profound yet unknown effect on the DNA translocation (Figure S7). Much

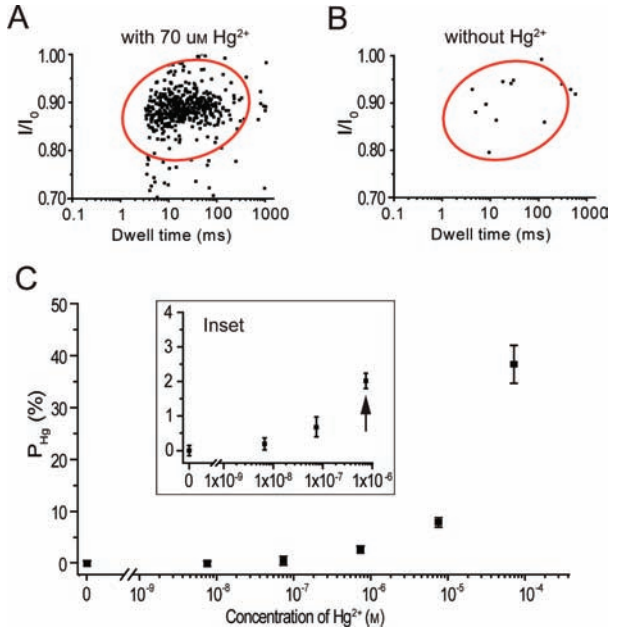

Figure 3. Quantification of Hg^{2+}. (A) Illustration of "Hg^{2+} signal region" specified by an oval with 95% confidence level. Note that data with current blockage smaller than 70% and duration shorter than 3 ms were truncated. The experiments were carried out in the buffer of 1 M KCl and 25 mM Tris, pH 8.0, at +100 mV, in the presence of 70 μM Hg^{2+} (DNA concentration 1.0 μM). (B) Generation of the Hg^{2+} signal oval in the control group (data truncated as (A), see Data Analysis section). (C) Plot of P_{Hg} versus Hg^{2+} concentration (number of individual experiments $n = 6$). The control group value has been offset to zero. The existence of Hg^{2+} can be confirmed at ~0.7 μM or higher.

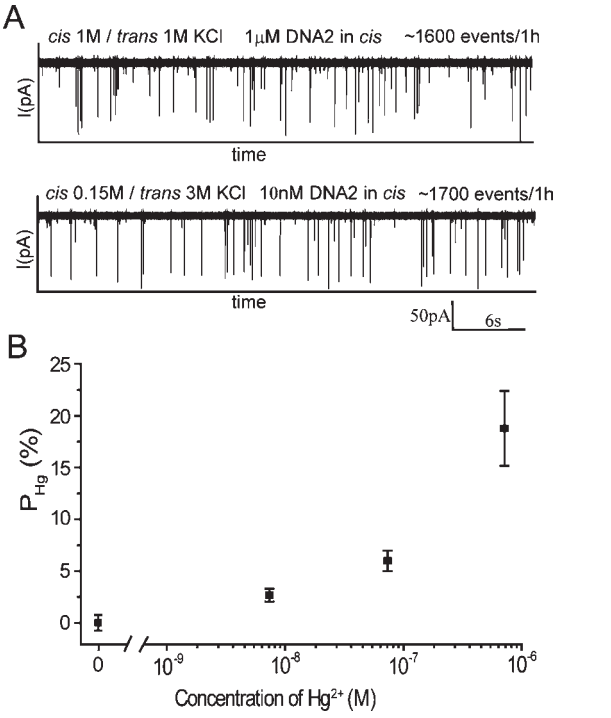

Figure 4. Detection of Hg^{2+} at low concentrations. (A) Comparison of the frequency of DNA translocation under symmetrical and asymmetric salt concentration conditions. (B) Plot of P_{Hg} versus Hg^{2+} concentration. Experiments were carried out with DNA2 (10 nM) in *cis* under 3 M *trans*/0.15 M *cis* KCl conditions. The control group value has been offset to zero (number of individual experiments $n = 5$). The existence of Hg^{2+} can be confirmed between ~7 and 700 nM range under the above conditions.

lower DNA capture rate and some extraordinarily long events were observed in 1 M KNO_3 under otherwise identical conditions. We also tried to thread DNA2 from *trans* to *cis* in the presence of Hg^{2+} in *trans* (Figure S8). Again, the frequency of DNA translocation was reduced to about 1/10 of that of *cis* to *trans* and the background noise also exists in the recordings. Finally, one strategy developed on solid-state nanopores attracted our attention. Meller et al. used a salt gradient to focus unlabeled DNA into nanopores, thus, drastically lowering the detection limit of DNA molecules.[33] We speculate that this strategy might also work on the protein nanopore system to improve the sensitivity. Interestingly, almost same frequency of DNA translocation events was observed for 10 nM DNA2 (*cis*) in a salt gradient of 3 M *trans*/0.15 M *cis* KCl compared with 1 μM DNA2 in 1 M *trans*/1 M *cis* KCl under optimized conditions (Figure 4A). DNA2 (1 μM) in 1 M *trans*/1 M *cis* KCl affords ~1600 events/h, while DNA2 (10 nM) in a salt gradient of 3 M *trans*/0.15 M *cis* KCl produces ~1700 events/h. Prompted by this result, we carried out three Hg^{2+} detection experiments at concentrations of 7, 70, and 700 nM, respectively. The results are shown in Figure 4B (for scatter plot data, see Figure S9). It is remarkable that with the asymmetric salt gradient conditions, the detection limit of Hg^{2+} could be lowered down to around 7 nM. The sensitivity of the sensor can be improved by about 2 orders of magnitude without adding any complexity to the sensing system. It should be noted that when DNA concentrations are above 100 nM under salt gradient conditions (*tran*/*cis* = 20/1), recordings of DNA translocation can be interrupted by frequent long-lived blockades, many of which require clearing by brief potential reversal. Thus, the asymmetric salt gradient is more suitable for detection of low concentration Hg^{2+} (~7−700 nM),

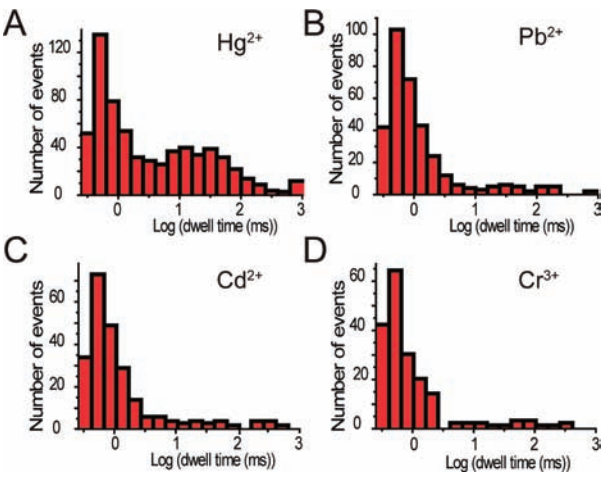

Figure 5. Histogram representation of DNA2 translocation in presence of 7 μM Hg^{2+} (A) or interfering metal ions Pb^{2+} (B), Cd^{2+} (C), and Cr^{3+} (D). Upon addition of Hg^{2+}, a noticeable peak appeared in the histogram, with a characteristic dwell time of ~10−30 ms. For either of Pb^{2+}, Cd^{2+}, and Cr^{3+}, no similar peak was observed. Data for other common metal ions are shown in Figure S10. Note that only events with current blockage over 70% and dwell time longer than 300 μs are selected. All experiments were performed at +100 mV in 1 M KCl and 25 mM Tris, pH 8.0 (DNA concentration 1.0 μM; number of individual experiments $n = 3$).

dx.doi.org/10.1021/ja206983z |J. Am. Chem. Soc. 2011, 133, 18312–18317

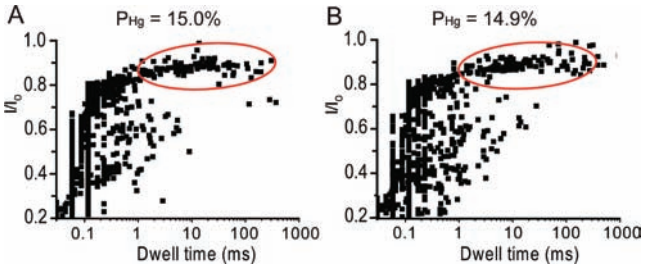

Figure 6. Detection of Hg^{2+} in the absence and presence of an analyte matrix. (A) Detection of 10.0 μM Hg^{2+} was carried out in the buffer of 1 M KCl and 25 mM Tris, pH 8.0, at +100 mV. The calculated P_{Hg} is 15.0% (B) An analyte matrix composed of Pb^{2+}, Cd^{2+}, Zn^{2+}, Cu^{2+}, Ca^{2+}, Mg^{2+}, Al^{3+}, Ni^{2+}, Ba^{2+}, and Fe^{3+} (final concentration of each metal ion is 100 μM) was mixed with Hg^{2+} for the detection experiments. The calculated P_{Hg} is 14.9%. The difference between the two P_{Hg} values is within experimental error range (DNA concentration 1.0 μM for all experiments; number of individual experiments n = 3).

while the symmetrical salt condition works better for detection of Hg^{2+} between 0.7 μM and 1 mM range.

Next, we investigated the selectivity of this sensing platform toward Hg^{2+}. Several metal ions with the final concentration of 7 μM were added to the assay and evaluated for selectivity. The results are shown as histograms of M^{n+}—DNA2 translocation in Figure 5 and Figure S10. It is apparent that the environmentally relevant metal ions such as Pb^{2+}, Cd^{2+}, Cr^{3+} and other common metal ions Zn^{2+}, Cu^{2+}, Ca^{2+}, Mg^{2+}, Ni^{2+}, Ba^{2+}, Al^{3+}, and Fe^{3+} (Figure S10) do not interfere with ssDNA2 translocation. To mimic a realistic sample in which the concentration of other metal ions might be higher than Hg^{2+}, we composed an analyte matrix by mixing Hg^{2+} and all other metal ions including Pb^{2+}, Cd^{2+}, Cr^{3+}, Zn^{2+}, Cu^{2+}, Ca^{2+}, Mg^{2+}, Ni^{2+}, Ba^{2+}, Al^{3+}, and Fe^{3+} which are 10 times concentrated and carried out the Hg^{2+} detection experiments under the standard conditions (Figure 6). The difference between the calculated P_{Hg} caused by the absence and presence of the analyte matrix is within experimental error range. Therefore, this DNA-based sensing device is highly selective for Hg^{2+} detection.

CONCLUSION

In summary, we have designed a mercury (Hg^{2+}) sensing platform based on the T—Hg^{2+}—T pairing using single-channel recording technique. The duplex formation mediated by Hg^{2+} in a properly chosen ssDNA generates a stable hairpin structure, which greatly alters the translocation profile of the ssDNA through αHL nanopore. The presence of Hg^{2+} can be confirmed in as little as 30 min at ~7 nM or higher. In the low concentration range, the sensitivity can be improved by employing asymmetric electrolyte gradients. The sensor can be fabricated from readily available materials, without the processes of synthesis, purification, probe-making, and so forth. Only wild-type αHL is required to form the nanopore, which is also a big advantage. The sensor is highly selective for Hg^{2+}, without interference from other metal ions. This sensing strategy opens new possibilities for detecting many types of analytes which have specific interactions with DNA molecules.

EXPERIMENTAL SECTION

Materials. All DNA samples (Table S1) were purchased from Tsingke Technologies (Beijing, China) and purified by PAGE. αHL Wildtype-D8H6 was produced by expression in BL21 (DE3) pLysS *Escherichia coli* cells and self-assembled into heptamers. 1,2-Diphytanoyl-*sn*-glycero-3-phosphocholine (DPhPc) was purchased from Avanti (Beijing). Barium chloride, manganese chloride tetrahydrate, calcium nitrate tetrahydrate, mercury(II) perchlorate trihydrate, zinc chloride, magnesium nitrate hexahydrate, aluminum chloride, nickel(II) nitrate hexahydrate, and cadmium perchlorate hexahydrate were obtained from Alfa Aesar. Copper(II) sulfate anhydrous and iron(III) nitrate nonahydrate were purchased from Sigma-Aldrich.

Buffer Preparation. A total of 7.455 g of KCl (99.999%, Sigma-Aldrich) and 0.394 g of Tris·HCl (99.0%, Sigma-Aldrich) were dissolved in ca. 80 mL of deionized water (Millipore, MA), followed by titration with concentrated NaOH (99.996%, J&K) until the pH of the solution was adjusted to 8.0. The solution was diluted with deionized water to 100 mL to obtain a buffer consisting of 1 M KCl and 25 mM Tris, pH 8.0.

Protein Preparation. αHL WT-D8H6 was expressed in the *E. coli* BL21 (DE3) pLysS strain, followed by purification through Ni column and oligomerization.[34] The monomer and heptamer proteins were separated by 8% SDS—PAGE and the heptamer band was cut from the gel. Mini protein gel extraction kit was used to extract the protein. The purified heptamer was conserved in buffer (10 mM Tris-HCl, pH 7.9, 50 mM NaCl) and stored at −70 °C.

Single-Channel Recording. All the recordings were carried out at 15 °C. 1,2-Diphytanoyl-*sn*-glycero-3-phosphocholine was used to form a bilayer on an aperture 100—150 μm in diameter in a 20-μm thick polytetrafluoroethylene film (Goodfellow, Malvern, PA). Each face of the polytetrafluoroethylene film was pretreated with 10% (v/v) hexadecane in pentane and both compartments were filled with 1 mL of buffer consisting of 1 M KCl and 25 mM Tris-HCl, pH 8.0. αHL heptamer and the mixture of DNA (final concentration 1 μM) and Hg^{2+} or other ions (final concentration 7 μM unless otherwise stated) were added to the *cis* compartment which was connected to ground. For asymmetric salt concentration experiments, DNA concentration is 10 nM and KCl concentration in *cis* is 0.15 M and in *trans* 3 M. The electrical current was detected with two Ag/AgCl electrodes, recorded with a patch-clamp amplifier (Axopatch 200B; Axon instruments, Foster City, CA), filtered with a low-pass Bessel filter with a corner frequency of 5 kHz, and then digitized with a Digidata 1440A A/D converter (Axon Instruments) at a sampling frequency of 20 kHz. The potential was held at +100 mV.

Hg^{2+} Detection Experiments. DNA samples (final concentration 1 μM) were incubated with various concentrations of Hg^{2+} (final concentrations 70, 7, 0.7, 0.07, 0.007 μM) or other metal ions (7 μM) for an hour at room temperature before use. Single-channel recordings were conducted on a patch-clamp amplifier.

Data Analysis. Current traces were analyzed with Clampfit 10.2 software (Axon Instruments). Events were detected using a threshold level that was 20% of the open-pore current. Origin and Clampfit were used for histogram construction, curve fitting and graph presentation. Generation of the Hg^{2+} signal oval from raw data: (1) cut off the data points with current blockages smaller than 70%; (2) remove the data points with duration shorter than 3 ms; (3) generate the "signal oval" using Origin 8.0. The function of the oval could be fitted by Matlab 7.1. With this function, the oval can be re-generated in the unedited data plot and the control group. Data points inside and outside the oval could be counted using this function.

ASSOCIATED CONTENT

Supporting Information. Supplemental table and figures. This material is available free of charge via the Internet at http://pubs.acs.org.

AUTHOR INFORMATION

Corresponding Author

zhaoyuliang@ihep.ac.cn; haichenwu@ihep.ac.cn

Author Contributions

‡These authors contributed equally.

ACKNOWLEDGMENT

This research was supported by 973 program (2010CB-933600), the National Natural Science Foundation of China (No. 20972159) and the "100 Talents" program of the Chinese Academy of Sciences. We are grateful to Prof. H. Bayley (Univ. of Oxford) for the plasmid of αHL.

REFERENCES

(1) Clarkson, T. W.; Magos, L.; Myers, G. J. *N. Engl. J. Med.* **2003**, *349*, 1731–1737.

(2) Davidson, P. W.; Myers, G. J.; Cox, C.; Axtell, C.; Shamlaye, C.; Sloane-Reeves, J.; Cernichiari, E.; Needham, L.; Choi, A.; Wang, Y. N.; Berlin, M.; Clarkson, T. W. *J. Am. Med. Assoc.* **1998**, *280*, 701–707.

(3) Wang, Q. R.; Kim, D.; Dionysiou, D. D.; Sorial, G. A.; Timberlake, D. *Environ. Pollut.* **2004**, *131*, 323–336.

(4) Grandjean, P.; Weihe, P.; White, R. F.; Debes, F. *Environ. Res.* **1998**, *77*, 165–172.

(5) Takeuchi, T.; Morikawa, N.; Matsumoto, H.; Shiraishi, Y. *Acta Neuropathol.* **1962**, *2*, 40–57.

(6) Onyido, I.; Norris, A. R.; Buncel, E. *Chem. Rev.* **2004**, *104*, 5911–5929.

(7) Harris, H. H.; Pickering, I. J.; George, G. N. *Science* **2003**, *301*, 1203.

(8) Tchounwou, P. B.; Ayensu, W. K.; Ninashvili, N.; Sutton, D. *Environ. Toxicol.* **2003**, *18*, 149–175.

(9) (a) Prodi, L.; Bargossi, C.; Montalti, M.; Zaccheroni, N.; Su, N.; Bradshaw, J. S.; Izatt, R. M.; Savage, P. B. *J. Am. Chem. Soc.* **2000**, *122*, 6769–6770. (b) Nolan, E. M.; Lippard, S. J. *J. Am. Chem. Soc.* **2003**, *125*, 14270–14271. (c) Guo, X. F.; Qian, X. H.; Jia, L. H. *J. Am. Chem. Soc.* **2004**, *126*, 2272–2273. (d) Ros-Lis, J. V.; Marcos, M. D.; Martinez-Manez, R.; Rurack, K.; Soto, J. *Angew. Chem.* **2005**, *44*, 4405–4407. (e) Mello, J. V.; Finney, N. S. *J. Am. Chem. Soc.* **2005**, *127*, 10124–10125. (f) Yoon, S.; Albers, A. E.; Wong, A. P.; Chang, C. J. *J. Am. Chem. Soc.* **2005**, *127*, 16030–16031. (g) Caballero, A.; Martinez, R.; Lloveras, V.; Ratera, I.; Vidal-Gancedo, J.; Wurst, K.; Tarraga, A.; Molina, P.; Veciana, J. *J. Am. Chem. Soc.* **2005**, *127*, 15666–15667. (h) Yang, Y. K.; Yook, K. J.; Tae, J. *J. Am. Chem. Soc.* **2005**, *127*, 16760–16761. (i) Zhu, X. J.; Fu, S. T.; Wong, W. K.; Guo, H. P.; Wong, W. Y. *Angew. Chem.* **2006**, *45*, 3150–3154. (j) Yoon, S.; Miller, E. W.; He, Q.; Do, P. H.; Chang, C. J. *Angew. Chem.* **2007**, *46*, 6658–6661. (k) Nolan, E. M.; Lippard, S. J. *J. Am. Chem. Soc.* **2007**, *129*, 5910–5918. (l) Jiang, W.; Wang, W. *Chem. Commun. (Cambridge, U.K.)* **2009**, 3913–3915.

(10) (a) Brummer, O.; La Clair, J. J.; Janda, K. D. *Org. Lett.* **1999**, *1*, 415–418. (b) Ros-Lis, J. V.; Martinez-Manez, R.; Rurack, K.; Sancenon, F.; Soto, J.; Spieles, M. *Inorg. Chem.* **2004**, *43*, 5183–5185. (c) Coronado, E.; Galan-Mascaros, J. R.; Marti-Gastaldo, C.; Palomares, E.; Durrant, J. R.; Vilar, R.; Gratzel, M.; Nazeeruddin, M. K. *J. Am. Chem. Soc.* **2005**, *127*, 12351–12356. (d) Huang, J. H.; Wen, W. H.; Sun, Y. Y.; Chou, P. T.; Fang, J. M. *J. Org. Chem.* **2005**, *70*, 5827–5832. (e) Nazeeruddin, M. K.; Di Censo, D.; Humphry-Baker, R.; Gratzel, M. *Adv. Funct. Mater.* **2006**, *16*, 189–194. (f) Tatay, S.; Gavina, P.; Coronado, E.; Palomares, E. *Org. Lett.* **2006**, *8*, 3857–3860.

(11) (a) Lee, J. S.; Han, M. S.; Mirkin, C. A. *Angew. Chem.* **2007**, *46*, 4093–4096. (b) Huang, C. C.; Yang, Z.; Lee, K. H.; Chang, H. T. *Angew. Chem.* **2007**, *46*, 6824–6828. (c) Li, D.; Wieckowska, A.; Willner, I. *Angew. Chem.* **2008**, *47*, 3927–3931. (d) Lin, Y. H.; Tseng, W. L. *Anal. Chem.* **2010**, *82*, 9194–9200.

(12) (a) Gao, X. Y.; Xing, G. M.; Yang, Y. L.; Shi, X. L.; Liu, R.; Chu, W. G.; Jing, L.; Zhao, F.; Ye, C.; Yuan, H.; Fang, X. H.; Wang, C.; Zhao, Y. L. *J. Am. Chem. Soc.* **2008**, *130*, 9190–9191. (b) Kim, T. H.; Lee, J.; Hong, S. *J. Phys. Chem. C* **2009**, *113*, 19393–19396. (c) Zhang, L. B.; Tao, L.; Li, B. L.; Jing, L.; Wang, E. K. *Chem. Commun.* **2010**, *46*, 1476–1478.

(13) (a) Chen, B.; Ying, Y.; Zhou, Z. T.; Zhong, P. *Chem. Lett.* **2004**, *33*, 1608–1609. (b) Xia, Y. S.; Zhu, C. Q. *Talanta* **2008**, *75*, 215–221. (c) Freeman, R.; Finder, T.; Willner, I. *Angew. Chem.* **2009**, *48*, 7818–7821.

(14) (a) Zhao, Y.; Zhong, Z. Q. *J. Am. Chem. Soc.* **2006**, *128*, 9988–9989. (b) Kim, I. B.; Bunz, U. H. F. *J. Am. Chem. Soc.* **2006**, *128*, 2818–2819. (c) Liu, X. F.; Tang, Y. L.; Wang, L. H.; Zhang, J.; Song, S. P.; Fan, C. H.; Wang, S. *Adv. Mater.* **2007**, *19*, 1662.

(15) (a) Kim, H. J.; Park, D. S.; Hyun, M. H.; Shim, Y. B. *Electroanalysis* **1998**, *10*, 303–306. (b) Nolan, M. A.; Kounaves, S. P. *Anal. Chem.* **1999**, *71*, 3567–3573.

(16) (a) Xu, X. H.; Thundat, T. G.; Brown, G. M.; Ji, H. F. *Anal. Chem.* **2002**, *74*, 3611–3615. (b) Cherian, S.; Gupta, R. K.; Mullin, B. C.; Thundat, T. *Biosens. Bioelectron.* **2003**, *19*, 411–416.

(17) Hollenstein, M.; Hipolito, C.; Lam, C.; Dietrich, D.; Perrin, D. M. *Angew. Chem.* **2008**, *47*, 4346–4350.

(18) Ono, A.; Togashi, H. *Angew. Chem.* **2004**, *43*, 4300–4302.

(19) Liu, J.; Lu, Y. *Angew. Chem.* **2007**, *46*, 7587–7590.

(20) Dave, N.; Chan, M. Y.; Huang, P. J. J.; Smith, B. D.; Liu, J. W. *J. Am. Chem. Soc.* **2010**, *132*, 12668–12673.

(21) Braha, O.; Gu, L. Q.; Zhou, L.; Lu, X. F.; Cheley, S.; Bayley, H. *Nat. Biotechnol.* **2000**, *18*, 1005–1007.

(22) (a) Movileanu, L.; Howorka, S.; Braha, O.; Bayley, H. *Nat. Biotechnol.* **2000**, *18*, 1091–1095. (b) Cheley, S.; Xie, H. Z.; Bayley, H. *ChemBioChem* **2006**, *7*, 1923–1927.

(23) Howorka, S.; Cheley, S.; Bayley, H. *Nat. Biotechnol.* **2001**, *19*, 636–639.

(24) (a) Gu, L. Q.; Braha, O.; Conlan, S.; Cheley, S.; Bayley, H. *Nature* **1999**, *398*, 686–690. (b) Wu, H. C.; Bayley, H. *J. Am. Chem. Soc.* **2008**, *130*, 6813–6819. (c) Guan, X. Y.; Gu, L. Q.; Cheley, S.; Braha, O.; Bayley, H. *ChemBioChem* **2005**, *6*, 1875–1881.

(25) Siran, L.; Wen-Wu, L.; Rotem, D.; Mikhailova, E.; Bayley, H. *Nat. Chem.* **2010**, 921–928.

(26) (a) Shim, J. W.; Tan, Q. L.; Gu, L. Q. *Nucleic Acids Res.* **2009**, *37*, 972–982. (b) Ying, Y. L.; Wang, H. Y.; Sutherland, T. C.; Long, Y. T. *Small* **2011**, *7*, 87–94.

(27) (a) Wendell, D.; Jing, P.; Geng, J.; Subramaniam, V.; Lee, T. J.; Montemagno, C.; Guo, P. X. *Nat. Nanotechnol.* **2009**, *4*, 765–772. (b) Maglia, G.; Restrepo, M. R.; Mikhailova, E.; Bayley, H. *Proc. Natl. Acad. Sci. U.S.A.* **2008**, *105*, 19720–19725. (c) Stoddart, D.; Heron, A. J.; Mikhailova, E.; Maglia, G.; Bayley, H. *Proc. Natl. Acad. Sci. U.S.A.* **2009**, *106*, 7702–7707. (d) Jing, P.; Haque, F.; Shu, D.; Montemagno, C.; Guo, P. X. *Nano Lett.* **2010**, *10*, 3620–3627. (e) Jing, P.; Haque, F.; Vonderheide, A. P.; Montemagno, C.; Guo, P. X. *Mol. BioSyst.* **2010**, *6*, 1844–1852. (f) Geng, J.; Fang, H. M.; Haque, F.; Zhang, L.; Guo, P. X. *Biomaterials* **2011**, *32*, 8234–8242.

(28) Sauer-Budge, A. F.; Nyamwanda, J. A.; Lubensky, D. K.; Branton, D. *Phys. Rev. Lett.* **2003**, *90*, 238101.

(29) Mathe, J.; Visram, H.; Viasnoff, V.; Rabin, Y.; Meller, A. *Biophys. J.* **2004**, *87*, 3205–3212.

(30) Meller, A.; Nivon, L.; Branton, D. *Phys. Rev. Lett.* **2001**, *86*, 3435–3438.

(31) Meller, A.; Nivon, L.; Brandin, E.; Golovchenko, J.; Branton, D. *Proc. Natl. Acad. Sci. U.S.A.* **2000**, *97*, 1079–1084.

(32) Dove, A. *Aquat. Ecosyst. Health Manage.* **2009**, *12*, 281–295.

(33) Wanunu, M.; Morrison, W.; Rabin, Y.; Grosberg, A. Y.; Meller, A. *Nat. Nanotechnol.* **2010**, *5*, 160–165.

(34) Bhakdi, S.; Fiissle, R.; Tranum-Jensen, J. *Proc. Natl. Acad. Sci. U.S.A.* **1981**, *78*, 5475–5479.